$$\delta z_{\mathrm{u}} = \nu_{\mathrm{u}}\varepsilon_1 h \tag{3}$$

where ν_{u} is the Poisson's ratio of the undrained material. As time proceeds and the pore pressure gradients caused by the earthquake are dissipated, the volume of rock will eventually reach a drained state. The residual subsidence after complete hydrostatic re-equilibrium of pore pressure is

$$\delta z_{\mathrm{d}} = \nu_{\mathrm{d}}\varepsilon_1 h \tag{4}$$

where ν_{d} is the Poisson's ratio of the drained material. Because ν_{u} is larger than ν_{d} (*15*), postseismic adjustment of pore pressure in the pull-apart results in surface upheaval

$$u = (\nu_{\mathrm{u}} - \nu_{\mathrm{d}})\varepsilon_1 h \tag{5}$$

Conversely, if coseismic strain produced local compression of a volume of rock, the coseismic deformation would produce uplift and the postseismic flow of pore fluid would cause subsidence. Such a process would explain the observed subsidence in the restraining bend along the Emerson fault (profile 1, Figs. 1 and 2).

Typical values for the Poisson's ratios of drained and undrained materials yield $\nu_{\mathrm{u}} - \nu_{\mathrm{d}} = 0.03$ (*15*). Assuming that $\delta l = 3$ m [as estimated across the Homestead Valley pull-apart (*10*)], $l = 5$ km, and $h = 4$ km, Eq. 5 gives a postseismic uplift $u = 7$ cm. The amount of uplift increases linearly with the porosity and thickness of the layer and decreases as the Poisson's ratio of the pristine rock increases, such that a trade-off exists between these parameters. However, the calculation shows that the use of reasonable values for these parameters yields a few centimeters of postseismic uplift, consistent with the radar data.

We thus conclude that pore fluid transfer provides a plausible mechanism to account for postseismic rebound in fault step-overs. Our model accounts both for postseismic subsidence in compressive jogs and uplift in pull-apart structures (*16*). The relaxation times involved in pore fluid flow processes (*2*, *17*) and the modeled amplitude of vertical surface adjustments are consistent with the observed decay rate and amplitude of postseismic surface movements in the step-overs of the 1992 Landers break. A critical test of this model would require pore pressure data that can be obtained by water-level measurement in wells near rupture zones. Such data are lacking in the region of Landers.

REFERENCES AND NOTES

1. For example, see Z. K. Shen *et al.*, *Bull. Seismol. Soc. Am.* **84**, 780 (1994); F. K. Wyatt, D. C. Agnew, M. Gladwin, *ibid.*, p. 768.
2. A. Nur and J. R. Booker, *Science* **175**, 885 (1972).
3. K. W. Hudnut, L. Seeber, J. Pacheco, *Geophys. Res. Lett.* **16**, 199 (1989).
4. J. R. Booker, *J. Geophys. Res.* **79**, 2037 (1974); C. H. Scholz, *Geology* **2**, 551 (1974); J. B. Rundle and W. Thatcher, *Bull. Seismol. Soc. Am.* **70**, 1869 (1980).
5. GPS arrays in the region of Landers have station spacing of ~10 km or more and therefore capture only long-wavelength features of the deformation field (*1*). Small-aperture trilateration arrays were surveyed after the earthquake and were able to measure only minor, localized deformation along the 1992 rupture [A. G. Sylvester, *Geophys. Res. Lett.* **20**, 1079 (1993)]. Creepmeters along the Eureka Peak fault revealed up to 23 cm of surface slip in 1 year [J. Behr *et al.*, *Bull. Seismol. Soc. Am.* **84**, 826 (1994)].
6. H. Gabriel, R. Goldstein, H. Zebker, *J. Geophys. Res.* **94**, 9183 (1989); H. Zebker *et al.*, *ibid.* **99**, 19617 (1994); G. Peltzer and P. Rosen, *Science* **268**, 1333 (1995).
7. We used the three-pass method to process SAR data acquired by the European remote sensing satellite (ERS-1) into interferograms (*6*). Each SAR image triplet forms a pair of images spanning a long time interval with a small spatial baseline (*6*) and a pair spanning a short time interval to remove the topographic phase signal. The data were acquired on descending orbits on (A) 7 August 1992–24 September 1995–11 June 1995, (B) 27 September 1992–23 January 1996–14 November 1995, and (C) 10 January 1993–23 May 1995–14 November 1995. For each image triplet, the first two dates correspond to the long time interval pair and the last two dates to the pair used to remove the topography.
8. Surface strain patterns of longer wavelength are also clear in the intermediate field and are the subject of a separate study (G. Peltzer *et al.*, in preparation).
9. K. Sieh *et al.*, *Science* **260**, 171 (1993); E. W. Hart *et al.*, *California Geol.* **46**, 10 (1993).
10. J. M. Sower *et al.*, *Bull. Seismol. Soc. Am.* **84**, 528 (1994); J. A. Spotila and K. Sieh, *J. Geophys. Res.* **100**, 545 (1995).
11. A. Sylvester, personal communication.
12. For ERS-1, the satellite line of sight is nearly perpendicular to the orbit and has an incidence angle of 23° in the center of the scene [European Space Agency, *ERS-1 System* (ESA Publications Division, ESTEC, Noordwijk, Netherlands, 1992)].
13. See, for example, K. Mogi, *Tokyo Univ. Earthquake Res. Inst. Bull.* **40**, 107 (1962); P. J. Eaton, *U.S. Geol. Surv. Prof. Pap. 579* (1967).
14. D. L. Anderson and J. H. Whitcomb, *J. Geophys. Res.* **80**, 1497 (1975); R. Muir-Wood and G. C. P. King, *J. Geophys. Res.* **98**, 22035 (1993).
15. J. K. MacKenzie [*Proc. Phys. Soc. London Sect. B* **63**, 1 (1950)] derived the elastic constants for a solid containing spherical holes, and Y. Sato [*Tokyo Univ. Earthquake Res. Inst. Bull.* **30**, 178 (1952)] extended the study to solids with holes filled with a fluid. Assuming a porosity of 2%, a Poisson's ratio of 0.27 for the solid, and the compressibility of the pore fluid to be equal to that of the solid, Sato's equations 3.2 and 3.3 give the Poisson's ratios of the drained material $\nu_{\mathrm{d}} = 0.268$ and the undrained material $\nu_{\mathrm{u}} = 0.278$ (note that $\nu_{\mathrm{d}} < \nu_{\mathrm{u}}$). These values are within the range of the values listed by J. R. Rice and M. P. Cleary [*Rev. Geophys. Space Phys.* **14**, 227 (1976)], estimated from laboratory tests for a variety of crustal materials. If the values listed for charcoal granite—which has a Poisson's ratio of 0.27, close to the ratio of 0.29 estimated from *P*-wave velocities for the upper crust in the Mojave Desert [Y. G. Li, L. T. Henyey, P. C. Leary, *J. Geophys. Res.* **97**, 8817 (1992)]—are representative of crustal materials at Landers, then $\nu_{\mathrm{d}} = 0.27$ and $\nu_{\mathrm{u}} = 0.30$. We assume $\nu_{\mathrm{u}} - \nu_{\mathrm{d}} = 0.03$ for the present calculation, although large uncertainties clearly exist for these values.
16. An alternative model involving fault collapse and fault strike perpendicular compression has been advocated to explain surface uplift near the Johnson Valley fault [D. Massonnet, W. Thatcher, H. Vadon, *Nature* **382**, 612 (1996)]. Although fault strike perpendicular compression may have actually occurred after the 1992 Landers earthquake, such a model does not explain the fact that the observed strain is localized in fault step-overs and is not distributed along the entire 1992 rupture, nor does it explain the subsidence observed in the compressive jog along the Emerson–Camp Rock fault.
17. Given a length scale of 10 km, the calculated relaxation time of 270 days yields a hydraulic diffusivity on the order of 10^4 cm^2 s^{-1}, consistent with the value estimated for a variety of earthquake-associated phenomena (*14*).
18. We thank E. Ivins and P. Segall for discussions on postseismic deformation processes, A. Sylvester for sharing unpublished results of leveling across the Homestead Valley fault, and two anonymous reviewers for constructive suggestions. The ERS-1 radar data were provided by the European Space Agency. The research described in this paper was carried out at the Jet Propulsion Laboratory, California Institute of Technology, under contract with NASA, and at the U.S. Geological Survey.

4 June 1996; accepted 17 July 1996

The Metabolic Status of Some Late Cretaceous Dinosaurs

John A. Ruben,* Willem J. Hillenius, Nicholas R. Geist,
Andrew Leitch, Terry D. Jones, Philip J. Currie,
John R. Horner, George Espe III

Analysis of the nasal region in fossils of three theropod dinosaurs (*Nanotyrannus, Ornithomimus,* and *Dromaeosaurus*) and one ornithischian dinosaur (*Hypacrosaurus*) showed that their metabolic rates were significantly lower than metabolic rates in modern birds and mammals. In extant endotherms and ectotherms, the cross-sectional area of the nasal passage scales approximately with increasing body mass M at $M^{0.72}$. However, the cross-sectional area of nasal passages in endotherms is approximately four times that of ectotherms. The dinosaurs studied here have narrow nasal passages that are consistent with low lung ventilation rates and the absence of respiratory turbinates.

Knowledge of dinosaur metabolic physiology can help improve understanding of their feeding and reproductive habits, as well as their routine modes of existence. Similarly, because birds are probably descendants (*1*) or near relatives of dinosaurs

(2), insight into dinosaur metabolism is likely to yield valuable clues to the evolution of endothermy in birds. However, anatomical structures that are causally linked with ecto- or endothermic metabolism in living tetrapods and thus could be particularly helpful in interpreting the metabolic status of extinct taxa are usually composed of soft tissues that are unlikely to fossilize (such as four-chambered hearts, complex lungs, and so on). Consequently, deciphering the metabolic status of dinosaurs has traditionally been limited to divining attributes putatively correlated with, but not necessarily causally linked with, maintenance of either low or high metabolic rates [such as fossil bone oxygen isotopic composition, growth rates, and bone histology (3)] Certainly their sheer mass probably enabled many dinosaurs to be bulk homeotherms (4), but paleontological evidence for dinosaur metabolic rates has been equivocal at best (3, 5).

The presence or absence of nasal respiratory turbinates in fossilized tetrapods may be used to infer the metabolic status of long-extinct groups (6). Here we present evidence that respiratory turbinates and other nasal passage modifications associated with endothermic rates of lung ventilation were absent in a variety of theropod dinosaurs and in at least one group of ornithopod ("duckbill") dinosaurs.

Respiratory turbinates (respiratory conchae) are epithelially lined, scroll-like, ossified or cartilaginous structures located in the anterior nasal passages of more than 99% of all extant birds and mammals (Fig. 1 and Fig. 2, B and C); their presence increases the surface area of the nasal passage. During inhalation and exhalation, respiratory turbinates act as intermittent countercurrent heat exchangers. By this process, they function to reduce the otherwise dramatically accelerated rates of respiratory evaporative heat and water loss that would accompany the high lung ventilation rates typical of endothermic taxa (7–9). Embryological studies indicate that the overall anatomical similarity of respiratory turbinates in birds and mammals is a product of convergent evolution; that is, these structures are likely to have evolved independently in mammalian and avian lineages (10). In contrast, respiratory turbinates are universally absent in extant ectothermic tetrapods. Field metabolic and lung ventilation rates in ectotherms are only about 5% of those of similarly sized endotherms (11) and are less likely to be associated with accelerated rates of respiratory loss of water and heat.

Together these observations suggest that the transition to high metabolic and lung ventilation rates in both protobirds and protomammals was probably accompanied by the independent, concurrent evolution of respiratory turbinates. Similarly, expansion of the nasal cavity to accommodate the presence of respiratory turbinates might also be expected to have occurred during the evolution of endothermy. Accordingly, the presence of respiratory turbinates and enlarged nasal passages in fossil taxa can serve as causally linked indicators of elevated lung ventilation rates and, by extension, of high routine metabolic rate. In extinct forms, the absence of respiratory turbinates and of nasal passage modifications associated with them is a likely indicator that metabolic and lung ventilation rates were sufficiently low that evaporative respiratory loss of heat and water was not a problem (6, 8). Evidence for the existence of incipient respiratory turbinates has previously been described in therocephalian therapsids, which are Late Paleozoic taxa not far removed from the ancestry of mammals (6).

The nasal passage in extant archosaurs and mammals consists of an anterior vestibular region, typically adjacent to the nostrils. Immediately posterior to the vestibule

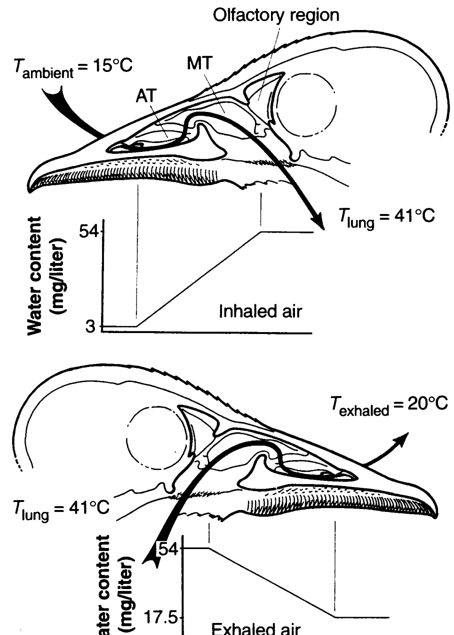

Fig. 1. The mechanism of respiratory turbinate function in modern endotherms. During inhalation (top), moist respiratory turbinate surfaces function to warm and humidify ambient air as it traverses the nasal passage. These same processes result in substantial cooling of respiratory turbinate surfaces. Upon exhalation (bottom), the process is reversed: Warm, moist exhaled air passes over the cooled surfaces of the respiratory turbinates. Exhaled air temperature is thereby reduced and water vapor condenses on respiratory turbinate surfaces. The result is a substantial reduction in the rate of respiratory loss of water and heat that would otherwise accompany high lung ventilation rates associated with endothermy (7, 8). Abbreviations: *T*, temperature; AT, anterior respiratory turbinate; MT, middle respiratory turbinate.

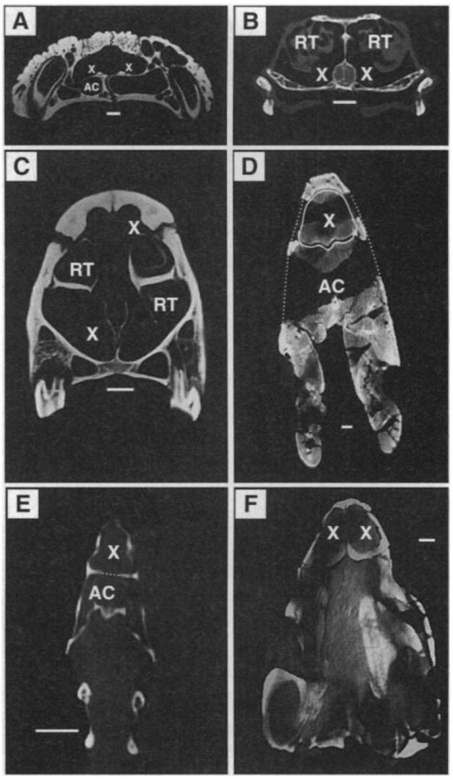

Fig. 2. Cross-sectional CAT scans of the nasal passage in (**A**) a crocodile (*Crocodylus*), (**B**) an ostrich (*Struthio*), (**C**) a bighorn sheep (*Ovus*), (**D**) the tyrannosaurid theropod dinosaur *Nanotyrannus*, (**E**) the ostrichlike theropod dinosaur *Ornithomimus*, and (**F**) the lambeosaurine duckbill dinosaur *Hypacrosaurus*. Respiratory turbinates in mammals and birds are housed in voluminous nasal passageways (see also Fig. 3). As in the alligator, the tubelike nasal passage (cavum nasi proprium) in these theropod dinosaurs appears to have been housed primarily within the maxillary and nasal bones. The main nasal passage in duckbill dinosaurs was probably an elongated nasal vestibulum, contained largely within the nasal bone (17). Some minimal postdepositional distortion of these fossils is evident. Nevertheless, the relatively narrow nasal passages in the dinosaurs indicate that, as suggested by their fossils, respiratory turbinates were probably absent in the living animals. Scale bar, 1 cm. Abbreviations: AC, accessory cavity; RT, respiratory turbinate; X, nasal passage proper.

J. A. Ruben, N. R. Geist, T. D. Jones, Department of Zoology, Oregon State University, Corvallis, OR 97331–2914, USA.

W. J. Hillenius, Biology Department, University of California, Los Angeles, CA 90024, USA.

A. Leitch, PaleoImage, Toronto, Ontario M8Z 5Z8, Canada.

P. J. Currie, Tyrrell Museum of Palaeontology, Drumheller, Alberta T0J 0Y0, Canada.

J. R. Horner, Museum of the Rockies, Montana State University, Bozeman, MT 59717, USA.

G. Espe III, The Salem Hospital, Salem OR 97301, USA.

*To whom correspondence should be addressed.

is the nasal cavity proper (cavum nasi proprium); the boundary between the two is usually denoted by ostia through which various nasal gland ducts communicate with the nasal passage. The nasal cavity proper is broadly subdivided into a main respiratory passageway and a "blind" posterodorsal or posterolateral olfactory region. Posteriorly, the nasal passage is continuous with the nasopharyngeal duct. In addition, a variety of pneumatized cranial cavities (sinuses) communicate with portions of the nasal passage in many amniotes (*10*).

Cartilaginous or osseous conchae (or turbinates) lined with olfactory sensory epithelia are housed within the olfactory regions of the nasal passage. Additionally, in birds and mammals, sheets of osseous or cartilaginous, often coiled, respiratory turbinates (the middle turbinates of birds and the maxilloturbinates of mammals) project into the nasal cavity proper (Fig. 2, B and C). Respiratory turbinates are oriented with their long axis parallel to the main path of airflow and are lined with well-vascularized respiratory epithelia. Birds generally possess an additional, anterior set of respiratory turbinates located within the rostral vestibular region (*10*).

In crocodilians, the perimeter of the tubelike nasal passage is bounded laterally and ventrally by thin medial processes from the premaxillary and maxillary bones; the roof of the passage is formed largely by the nasal bone (Fig. 2A). The boundaries of the mammalian nasal passage are typically well-defined by the nasal, premaxillary, and maxillary bones (Fig. 2C). The nasal passage proper is poorly ossified in most birds (Fig. 2B).

Expansion of the nasal cavity is necessary to accommodate the presence of respiratory turbinates, as well as to facilitate increased lung ventilation rates in endotherms. Consequently, it is to be expected that most birds and mammals might possess nasal passageways with markedly larger cross-sectional areas than those of ectotherms of equivalent mass. Regressions for this variation in endotherm-ectotherm anatomy (Fig. 3) indicate that nasal passage cross-sectional area in birds and mammals is about four times that of a number of similarly sized modern reptiles.

Computed axial tomography (CAT) scans from the mid-snout regions of superbly preserved specimens of the Late Cretaceous theropod dinosaurs *Nanotyrannus* (Tyrannosauridae) and *Ornithomimus* (Ornithomimidae) reveals that their anterior nasal anatomy was like that of modern crocodilians. These dinosaurs had a narrow, tubelike nasal passage bounded laterally and ventrally by medial processes of the maxillary bone and dorsally by the nasal bone (Fig. 2, D and E, and Fig. 4). There is no trace of respiratory turbinates in the nasal

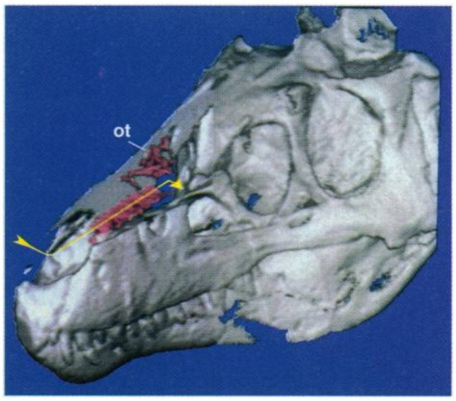

Fig. 4. The tubelike nasal passage of the tyrannosaurid dinosaur *Nanotyrannus*. The floor of the nasal passage was formed by medial processes of the maxillary bone, much as it is in modern crocodilians (Fig. 2, A and D). The yellow arrow marks the probable path of inhaled air through the nasal passage proper, moving ventrally into the nasopharyngeal region, posterior to the bony secondary palate (not shown in figure). Pink areas indicate the floor of the nasal passage. Abbreviation: ot, olfactory turbinate.

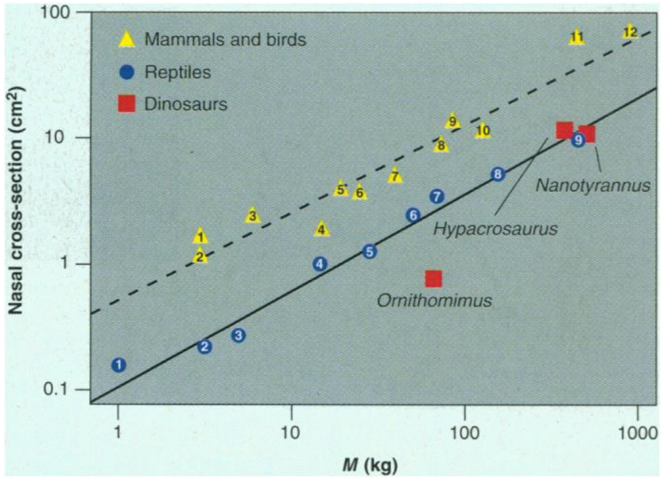

Fig. 3. The relation of nasal passage (cavum nasi proprium) cross-sectional area to body mass (*M*) in modern endotherms (mammals and birds), modern reptiles (lizards and crocodilians), and three genera of Late Cretaceous dinosaurs (*15*) (values for dinosaurs were not included in regression calculations). For mammals and birds, nasal cross section equals 0.57 $M^{0.68}$; SE = 0.358. For reptiles, nasal cross section equals 0.11 $M^{0.76}$; SE = 0.239. Numbers in yellow triangles indicate the following mammals and birds: 1, coatimundi (*Nasua*, 3 kg) and opossum (*Didelphis*, 3 kg); 2, great blue heron (*Ardea*, 3 kg); 3, raccoon (*Procyon*, 6 kg); 4, giant anteater (*Myrmecophaga*, 15 kg); 5, rhea (*Rhea*, 20 kg); 6, coyote (*Canis*, 25 kg); 7, emu (*Dromaius*, 40 kg); 8, human (75 kg); 9, black bear (*Ursus*, 85 kg); 10, ostrich (*Struthio*, 125 kg); 11, horse (*Equus*, 450 kg); and 12, African cape buffalo (*Syncerus*, 900 kg). Numbers in blue circles indicate the following reptiles: 1, false iguana (*Ctenosaura*, 1 kg); 2, monitor lizard (*Varanus*, 3 kg); 3, monitor lizards (*Varanus*, 4.8 kg and 5.0 kg); 4, crocodile (*Crocodylus*, 15 kg); 5, monitor lizard (*Varanus*, 28 kg); 6, alligator (*Alligator*, 70 kg); 7, crocodile (*Crocodylus*, 50 kg); 8, alligator (*Alligator*, 160 kg); and 9, crocodile (*Crocodylus*, 450 kg). Dinosaur masses, estimated from head or body skeletal length or both (*16*) are as follows: ostrich dinosaur *Ornithomimus* (Theropoda: Ornithomimidae), 65 kg (Campanian Stage; Tyrrell Museum of Palaeontology specimen 95.110.1); duckbill dinosaur *Hypacrosaurus* (Ornithischia: Hadrosauridae), 375 kg (Maastrichtian Stage; American Museum of Natural History specimen 5461); and tyrannosaurid dinosaur *Nanotyrannus* (Theropoda: Tyrannosauridae), 500 kg (Maastrichtian Stage; Cleveland Museum of Natural History specimen 7541).

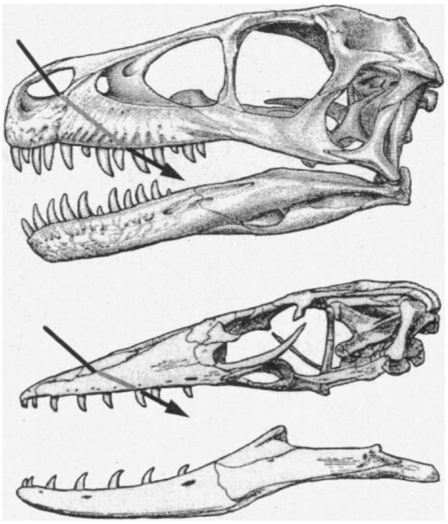

Fig. 5. Lateral views of the skulls of the of the maniraptoran theropod dinosaur *Dromaeosaurus* (Theropoda: Dromaeosauridae) (top) and the monitor lizard *Varanus* (Squamata: Varanidae) (bottom). The arrow shows the path of airflow through the nasal region into the oral cavity. In *Dromaeosaurus*, and probably in some other dromaeosaurid dinosaurs [such as *Deinonychus* (*13*)], the short direct path of airflow into the oral cavity was similar to that in *Varanus* (and many other extant lizards) and almost certainly precluded sufficient space to house respiratory turbinates {for *Dromaeosaurus* [figure modified from (*12*)], the presumed airflow route is based on the location of the nostrils and the anterior position of the vomer}. Dromaeosaurid dinosaurs are often assumed to be the sister group of birds (*18*).

passageways of these specimens. Additionally, because values for cross-sectional areas of the theropod nasal passages lie on or below the reptilian allometric regression (Fig. 3), respiratory turbinates were probably also absent in life. Similarly, CAT scans from a particularly well-preserved skull of the ornithischian dinosaur *Hypacrosaurus* (Ornithopoda: Hadrosauridae) also show no evidence of the presence of respiratory turbinates (Fig. 2F). Nasal cross sectional area in *Hypacrosaurus* is also coincident with the reptilian allometric regression (Fig. 3).

The proximity of the nostrils to the choanae (internal nares) in the maniraptoran theropod *Dromaeosaurus* (Dromaeosauridae) (*12*) and probably in *Deinonychus* (Dromaeosauridae) (*13*) as well is reminiscent of nasal cavity proportions in a variety of modern lizards (Varanidae, for example) (Fig. 5) (*14*). As in extant lizards, the abbreviated nasal passage associated with such a direct path of airflow into the oral cavity of these dinosaurs almost certainly precluded sufficient space in the nasal cavity to have accommodated respiratory turbinates.

Together the data indicate that a variety of Cretaceous theropod dinosaurs, and at least one genus of ornithischian dinosaurs, possessed crocodile- or lizardlike, relatively constricted nasal passages, devoid of sufficient cross-sectional area to have accommodated respiratory turbinates and endothermic lung ventilation rates. These observations do not necessarily either preclude or support the possibility that some or all of the taxa investigated here maintained routine metabolic rates somewhat greater than those of extant ectotherms.

REFERENCES AND NOTES

1. J. H. Ostrom, in *The Dinosauria*, D. B. Weishampel, P. Dodson, H. Osmolka, Eds. (Univ. of California Press, Berkeley, CA, 1990), pp. 269–279.
2. A. Feduccia, *Naturwissenschaften* **80**, 564 (1993).
3. J. A. Ruben, *Annu. Rev. Physiol.* **57**, 69 (1995); J. F. Hubert *et al.*, *J. Sediment. Res.* **66**, 531 (1996).
4. J. R. Spotila, M. P. O'Connor, F. V. Paladino, *Mod. Geol.* **16**, 203 (1991).
5. J. O. Farlow, P. Dodson, A. Chinsamy, *Annu. Rev. Ecol. Syst.* **26**, 445 (1995).
6. W. J. Hillenius, *Evolution* **48**, 207 (1994).
7. ———, *Paleobiol.* **18**, 117 (1992).
8. J. A. Ruben, in *Animals and Temperature*, I. A. Johnston and A. F. Bennett, Eds. (Cambridge Univ. Press, London, in press).
9. The rare exceptions in endotherms where respiratory turbinates are particularly poorly developed or absent are clearly related to secondary nasal or rostral specializations that preclude their presence. For example, turbinates and nostrils are absent in a number of diving birds of the order Pelecaniformes, including pelicans, gannets, and cormorants. Most of these birds are plunge divers and anterior open nostrils would be a potential liability in such cases [J. D. MacDonald, *Proc. Zool. Soc. London* **135**, 357 (1960)]. Similarly, respiratory turbinates are also absent or poorly developed in whales. However, in these exceptions, the presence of compensatory mechanisms serves to emphasize that endothermic lung ventilation rates necessitate some adaptation in order to counteract loss of respiratory water or heat {pelecaniformid birds maintain large nasal salt glands that probably allow them to drink sea water directly [P. C. Withers, *Comparative Animal Physiology* (Saunders College Press, Fort Worth, TX, 1992)]; at least some cetaceans possess a specialized nasal-cavity air compression mechanism for reduction of respiratory water and heat loss [W. H. Coulombe, S. H. Ridgeway, W. E. Elgin, *Science*, **149**, 86 (1965)]}.
10. L. M. Witmer, *J. Morphol.* **225**, 269 (1995).
11. K. A. Nagy and C. C. Peterson, *Ecol. Monogr.* **57**, 111 (1988).
12. P. J. Currie, *J. Vertebr. Paleontol.* **15**, 576 (1995).
13. J. H. Ostrom, *Bull. Am. Mus. Nat. Hist.* **30**, 1 (1969).
14. T. S. Parsons, in *Biology of the Reptilia*, C. Gans, d'A. Bellairs, T. S. Parsons, Eds. (Academic Press, New York, 1970), vol. 2, pp. 99–191.
15. Nasal cross-sectional areas were determined by means of microcomputer image analysis (MCID, Imaging Research, St. Catherines, Ontario, Canada) either of cranial CAT-scan imagery or directly from sectioned skulls.
16. P. Dodson, personal communication.
17. D. B. Weishampel, *J. Paleontol.* **55**, 1046 (1981).
18. J. A. Gauthier, *Calif. Acad. Sci. Mem.* **8**, 1 (1986).
19. We thank R. Aldred; P. Beardsley; V. Buchouse; P. Constant; S. Hamilton; M. Mason; A. Stuempsl; S. Vondersaar; M. Woo; L. Yao; Children's Hospital, San Diego, CA; Good Samaritan Hosptial, Corvallis, OR; and Salem Hospital, Salem, OR, for CAT scanning; D. Auth for the loan of varanid specimens; A. Bennett, P. Dodson, and D. Weishampel for comments; B. Byrne, J. Melville, and P. Murtaugh for statistical advice; J. Farlow for review and comments; J. Joslin and C. Simpkins of the Washington Park Zoo for donation of the varanid specimen; M. Mauxpoux for image analysis; M. Meers for advice; F. Moore and C. Richardson for equipment and advice; R. Pickton for bird specimens; G. Smith and N. Smith for donation of emu specimens; G. Vaillancourt and D. Vaillancourt for donation of ostrich specimens; and the University of California, Los Angeles, Dickey Collection; the Los Angeles County Museum of Natural History; and the Department of Zoology at Oregon State University for specimens. Supported by NSF grant IBN-9420290 to W.J.H. and J.A.R.

24 May 1996; accepted 24 June 1996

Enforcing Coherent Evolution in Dissipative Quantum Dynamics

J. I. Cirac, T. Pellizzari, P. Zoller

The major obstacle to the preparation and manipulation of many-particle entangled states is decoherence due to the coupling of the system to the environment. A scheme to correct for the effects of decoherence and enforce coherent evolution in the system dynamics is described and illustrated for the particular case of the ion-trap quantum computer.

The preparation and manipulation of N-particle entangled states is fundamental to the investigation of basic aspects of quantum mechanics and is the basis of applications such as quantum computation, teleportation, cryptography, and spectroscopy (*1*, *2*). The major obstacle to the production of an entangled state in the laboratory is decoherence because the system couples to an environment. Suppressing environmental effects is thus essential to create entangled states in mesoscopic systems. This question is closely related to the problem of error correction in quantum computers (QC). In the following we adopt a language in which the manipulation of a system of particles is phrased as a computation in a QC. Such a device can be thought of as a system of spin-1/2 particles (qubits) with states $|0\rangle$ and $|1\rangle$. Any unitary (reversible) operation on the system of particles (that is, any computation) can be decomposed into a sequence of one-qubit or two-qubit gates, which are operations that involve one and two particles, respectively. Thus, any state (entangled or not) of the system can be generated if one can implement one- and two-qubit operations (*1*). The effects of decoherence correspond to errors in the computation.

The error correction schemes proposed so far have focused on preserving a given entangled state (memory errors) (*3*). We introduce a method to correct for the effects of decoherence in the dynamical process of preparation and modification of entangled states (gate errors). The proposed scheme is a first-order error correction that allows us to effectively square the number of gate operations relative to the uncorrected case. The motivation is that in quantum optical systems, entangled states are achieved by coupling qubits to another degree of freedom that in turn undergoes decoherence by coupling to a heat bath. For example, in the ion-trap QC (*4*), the qubits can be stored in long-lived atomic ground states (*5*) with decoherence time $\simeq$1000 s (*2*). Two-bit quantum gates are implemented by coupling the ions to the collective center-of-mass motion in the trap, which decoheres in a time $\simeq$1 ms (*5*). Thus, at least in present experiments, gate errors predominate.

We illustrate our scheme in the context of the ion-trap QC (*4*). We consider a specific model of decoherence that results from a linear Markovian coupling between the ion motion (phonons) and a reservoir at

---

Institut für Theoretische Physik, Universität Innsbruck, Technikerstraße 25, A-6020 Innsbruck, Austria.